

Microstructure of thin tantalum films sputtered onto inclined substrates: Experiments and atomistic simulations

J. Dalla Torre^{a)}

Service de Recherches de Métallurgie Physique, CEA-Saclay, 91191 Gif-sur-Yvette, France

G. H. Gilmer^{b)}

Lawrence Livermore National Laboratory, Livermore, California 94550

D. L. Windt

Columbia Astrophysics Laboratory, 550 West 120th Street, New York, New York 10027

R. Kalyanaraman

Department of Physics, CB 1105, Washington University, 1 Brookings Drive, Saint Louis, Missouri 63130

F. H. Baumann

Bell Laboratories, Lucent Technologies, 700 Mountain Avenue, Murray Hill, New Jersey 07974

P. L. O'Sullivan

SINTEF Applied Mathematics, Postboks 124, Blindern, N-0314 Oslo, Norway

J. Sapjeta

Bell Laboratories, Lucent Technologies, 700 Mountain Avenue, Murray Hill, New Jersey 07974

T. Díaz de la Rubia

Lawrence Livermore National Laboratory, Livermore, California 94550

M. Djafari Rouhani

LAAS-CNRS, 7 avenue du Colonel Roche, 31077 Toulouse cedex, France and Laboratoire de Physique des Solides-UMR5477 CNRS, Université Paul Sabatier, 31062 Toulouse cedex, France

(Received 5 November 2002; accepted 9 April 2003)

We have combined experiments and atomistic modeling in order to better understand the growth and structure of metal films deposited onto sidewalls of trenches and vias. Using x-ray reflectance, atomic force microscopy, and high-resolution transmission electron microscopy to characterize the microstructure and morphology of Ta films grown by magnetron sputtering onto inclined substrates, we find that films deposited at larger incidence angles tend towards columnar microstructure with high roughness and low density. We have used a three-dimensional Monte Carlo model (ADEPT) to simulate the growth process, under conditions close to those investigated experimentally. A binary collision model is included in the Monte Carlo deposition procedure to describe the interaction of energetic particles with the surface. Examination of the film microstructure and morphology resulting from the simulations indicates that the energetic impinging particles are necessary to produce film densities comparable to those found experimentally. By including these effects, we thus find good agreement between the simulations and the experimental results. © 2003 American Institute of Physics. [DOI: 10.1063/1.1579112]

I. INTRODUCTION

The control of thin film microstructure and morphology is important in many applications, particularly in metallization processes involved in the construction of interconnects on silicon. A typical example of this assertion is the so-called "barrier layer," i.e., a thin layer of a refractory material (e.g., Ta, TaN, TiN) used to prevent interdiffusion of Al or Cu with the underlying silicon or silicon oxide. Voids can dramatically reduce the effectiveness of the barrier by providing a path for rapid diffusion. Trench and via sidewalls are perhaps the most sensitive zones for penetration of barrier films because of the potential for low step coverage and, in the case

of high-aspect-ratio features in particular, the grazing deposition angles on the sidewalls which can facilitate void formation.¹

Much research has been devoted to the understanding of columnar growth in thin film deposition. A large number of experiments and theoretical investigations show that, for low surface mobility and particularly for deposition conditions at oblique incidence, the film exhibits a columnar morphology (see Ref. 2 for a review paper). Dirks and Leamy³ suggest a kinetic roughening mechanism that results in column formation: small surface depressions become deeper and grow as deposition proceeds because (a) they receive a smaller flux due to shadowing, in the case of impinging atoms arriving at large incident angles, and (b) low atomic mobility prevents atoms from moving to fill this depression (which would minimize surface energy).

^{a)}Electronic mail: jdallatorre@cea.fr

^{b)}Electronic mail: gilmer1@llnl.gov

The sputter gas pressure during growth also is known to affect film microstructure. In the sputtering process, sputter gas ions (most commonly Ar^+) are accelerated towards a polycrystalline target with energies of up to a few hundred electron volts. At low Ar pressure, sputtered target atoms as well as neutral Ar atoms reflected from the target can arrive at the surface of the growing film with significant kinetic energies. In the specific case of Ta deposition with 400 eV Ar ions, binary collision calculations indicate energies as high as ~ 100 eV for Ar and an average kinetic energy of 26 eV for Ta.⁴ At high Ar pressure, however, collisions tend to thermalize the gas phase so that the amount of kinetic energy delivered to the surface of the growing film by neutral Ar and Ta atoms is greatly reduced. The larger incident kinetic energies associated with lower Ar pressures tend to produce high density, smooth films.⁵

The microstructure that results in the case of sputtering is due to several atomistic mechanisms taking place between the impinging energetic Ar and Ta atoms and the surface adatoms. (1) An adatom or Ar ion can reflect at the surface or induce resputtering of the surface atoms. (2) An impinging atom arriving at grazing incidence on the surface can also diffuse over large distances (biased diffusion). Biased diffusion is the consequence of the attractive force exerted on the impinging atom by the surface, preventing a simple reflection. (3) The impinging atom can collide with a surface atom and induce its diffusion (kinetic energy assisted diffusion). All of these mechanisms have been observed in molecular dynamics simulations,^{6–9} but their effect on the film microstructure is not fully understood.

Several attempts have been made to model numerically the effects of particle collisions with surface atoms, using either molecular dynamics (MD) or kinetic Monte Carlo (MC) simulations. Some recent work^{10,11} treated the dependence of microstructure on processing conditions including substrate temperature, incident energy, or incident angle of the atoms. Since MD follows the detailed atomic trajectories, the simulated time scale can only reach microseconds (even for hyperdynamics techniques¹²) whereas periods of minutes or more are common in experiments. In order to simulate deposition of realistic film thicknesses, deposition rates are usually accelerated by many orders of magnitude, and adatom diffusion is essentially excluded, except for athermal processes. On the other hand, some MC models were developed to reproduce effects of the energetic collisions on the surface. Yang *et al.* use a two-step model where impinging atoms are first placed near their landing point, based on a momentum scheme, and a kinetic MC describes the subsequent diffusion.¹³ In the momentum scheme, deposited atoms undergo an initial displacement, and this produces film densities closer to experimental values. More recently, Wang and Clancy's MC model included atom sticking probability in the deposition procedure.¹⁴ The kinetic energy of the impinging atoms along the normal to the surface is computed and if this energy is lower than a threshold energy, the atom does not stick.

In this article, we present experimental and simulation results of Ta thin films grown by magnetron sputtering onto oxidized Si substrates. Our experimental investigation was

intended to quantify how the microstructure and morphology of the film changes over nonplanar topography. We varied the deposition angle and the Ar pressure in the chamber, and quantified the surface roughness and density using x-ray reflectometry and atomic force microscopy. The film microstructure was investigated using high resolution transmission electron microscopy as well. Our simulations were performed using ADEPT, a three-dimensional MC model. The model includes ballistic deposition from the sputter target with realistic angular distributions, binding energies, and surface diffusion. The angular distribution for the impinging atoms corresponds to a collimated beam produced by a target that subtends a small solid angle. A binary collision model simulates atomic displacements resulting from energetic impinging particles, and we have investigated the effects of these collisions on the film microstructure. We compare the simulated morphologies to the experimental results.

II. EXPERIMENTAL RESULTS: TANTALUM FILMS

A. Film growth and analysis

The experimental work was described in detail elsewhere,¹⁵ and we provide here only an outline of the methods. The films were grown by dc magnetron sputtering in argon (99.999% purity). The background pressure in the chamber prior to deposition was in the range 5×10^{-7} – 5×10^{-6} Torr. S-Gun cathodes using 1.85-in. diameter cylindrical targets of Ta (99.9% purity) are mounted in the base plate of the vacuum chamber. Substrates are mounted on a platen that faces downward, located 110 mm above the top surface of the target; film thickness is adjusted by varying the (computer-controlled) rotational velocity of the substrate platen as it travels over the cathode. An aperture located 95 mm above the target is used both to improve source collimation and coating uniformity. Ta thin films were grown on (unheated) Si(100) wafer sections ($\sim 1.4 \times 1.4$ cm²) having a thin (~ 20 – 30 Å) native oxide layer. The wafer sections were mounted on a holder consisting of trapezoidal blocks that are oriented at various angles (Ψ_m) relative to the direction of the sputter source in order to vary the average incidence angle of particles.¹⁵ Orientation angles of $\Psi_m = 0^\circ$ (i.e., horizontal), 30° , 60° , and 85° were used. The power applied to the cathode was fixed at 100 W; the cathode voltage was approximately 350 V, so that the average kinetic energy of Ar ions impinging on the target was 350 eV. The argon pressure in the chamber was fixed at either 2 or 10 mTorr; the deposition rates determined from the film thicknesses (0° orientation angles) deduced by x-ray reflectance measurements (described below) were 9.3 and 8.2 Å/s, respectively. Film thicknesses varied with substrate orientation, with thinner films obtained at larger orientation angles, as described below.

X-ray reflectance (XRR) measurements were performed using a $\text{Cu } K\alpha$ source and a two-circle goniometer. Fits to the XRR data, performed with the IMD software package,¹⁶ were used to determine the film thickness, surface roughness, density, and interface widths (i.e., resulting from interfacial roughness and/or diffuseness between the film and the sub-

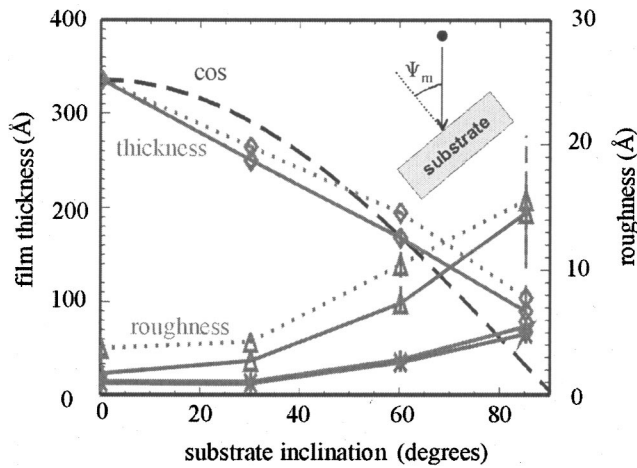


FIG. 1. Roughness values are determined as a function of orientation angle from XRR(Δ) and AFM with $1 \mu\text{m}$ (+) and $0.1 \mu\text{m}$ (\times) scan lengths. The thickness is measured from XRR(\diamond) and compared to $\cos(\Psi_m)$ (dashed line noted “cos” in the figure). Solid lines and dotted lines correspond to Ta films deposited, respectively, at 2 and 10 mTorr Ar pressure.

strate, and between the film and the oxide that forms during exposure to air).

Atomic force microscopy (AFM) was also used to determine surface roughness: measurements were made on selected films using a Digital Instruments Nanoscope III operated in the tapping mode, with both 1.0 and $0.1 \mu\text{m}$ scan lengths. Cross-sectional high resolution transmission electron microscopy (HRTEM) of the films was prepared by ion milling using 5 keV Ar at an angle of 15° from a dual ion mill (Gatan model 600) at liquid N_2 temperature. The cross-sectional pieces were glued such that the flux direction for growth of the Ta film lies in the polishing plane of the cross section. HRTEM was carried out using the 400 keV JEOL 4000EX high resolution electron microscope with a point-to-point resolution of 1.8 \AA .

B. Results of Ta film analysis

The thickness and roughness values determined from the x-ray data for the Ta films are plotted versus substrate orientation angle in Fig. 1. A number of trends are evident in these data:

First, the variation of thickness with orientation angle (Ψ_m) does not follow the $\cos \Psi_m$ distribution, as is often assumed.¹⁷ Part of this discrepancy can be due to imperfect source collimation, in spite of the use of the deposition aperture described in Ref. 15. Also, the density of the film varies with orientation, and this effect increases the thickness of the film grown at the more oblique angles.

Second, films deposited at high Ar pressure are rougher than those deposited at low Ar pressure. The variation of roughness with Ar pressure observed here is by now widely known to occur for sputtered films^{18–20} and results largely from the dependence of the deposition energetics on Ar pressure as discussed above.

Third, we observe an increase in roughness with orientation angle (Fig. 1), presumably related to columnar growth, which is enhanced at nonzero orientation angles as discussed

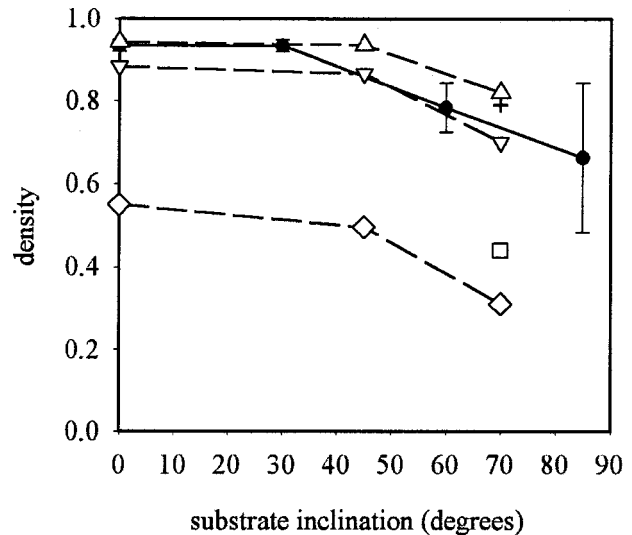


FIG. 2. XRR density measurement of Ta films deposited onto different inclined substrates (\bullet). These films have been deposited at $P_{\text{Ar}}=2 \text{ mTorr}$. Simulation results are also displayed for comparison: (\diamond): no energetics; (∇): $T(\text{Ta})=5 \text{ eV}$ and $T(\text{Ar})=25 \text{ eV}$; (Δ): $T(\text{Ta})=10 \text{ eV}$ and $T(\text{Ar})=50 \text{ eV}$; (+): $T(\text{Ta})=10 \text{ eV}$ and $T(\text{Ar})=0 \text{ eV}$; and (\square): latent heat.

above as well. In addition, the films exhibit an increase in roughness with substrate inclination for all measured values of the Ar pressure.

We plot the density as determined from XRR as a function of substrate orientation ($P_{\text{Ar}}=2 \text{ mTorr}$) in Fig. 2 (the simulation results are also displayed but are described in Sec. IV). The density decreases with inclination angle, from ~ 0.93 to ~ 0.66 (at 85° substrate inclination), that of the bulk crystalline material without voids (we use a full density of 16.6 g/cm^3). The low density determined from XRR correlates with the microstructure determined from HRTEM (Fig. 3) on the 60° inclination sample, which shows clearly an underdense film comprising columns less than 100 \AA wide, with no clear faceting on the top. A dense layer is also observed near the substrate. Note that large-angle x-ray diffraction measurements, also performed on selected samples, reveal no strong texture in these films.¹⁵

III. MONTE CARLO MODEL: ADEPT

ADEPT has been developed in order to describe the growth of metal films deposited by sputter deposition. The general features of ADEPT have been presented before,²¹ and we sketch here only the necessary background to understand the simulation procedure. The new binary collision model of the deposition procedure is presented in detail.

A. General simulation procedure

A typical simulation is a succession of deposition and surface diffusion events. The angular distribution for impinging particles is set to correspond to the geometry of the magnetron sputtering apparatus of the experiment:¹⁵ we use a collimated beam with trajectories that can differ by about 15° from an average angle (Ψ_m). The atom X and Y starting coordinates are randomly chosen above the substrate on top of the simulation cell. The impinging atom is moved along

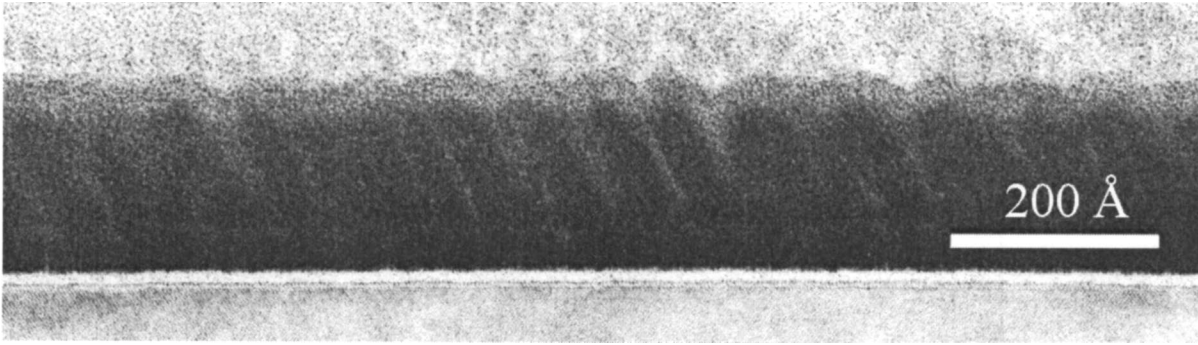


FIG. 3. HRTEM section of a Ta film grown on a 60° oriented substrate. The film has been grown under 2 mTorr Ar pressure.

the trajectory until it collides with the film surface. The average time between deposition events Δt_{depos} is derived from the desired deposition rate and the dimensions of the computational cell.

Surface diffusion is simulated in the model by selecting surface atoms and moving them to neighboring empty surface sites. The jump rate to the nearest neighbor empty site of the atoms with coordination <12 are temperature dependent and follow the Arrhenius form: $\nu = \nu_0 e^{-E_m/kT}$ where T is the temperature and k is the Boltzman constant. The prefactors ν_0 and the activation energies E_m are coordination dependant and can be inferred from MD calculations (in the initial implementations, MD simulations of Al provided the diffusion barriers²²). Surface atoms are picked with probabilities based on their maximum possible rates, which are determined by their coordination. The potential energies in the initial and final positions of a diffusion jump are calculated using a Monte Carlo embedded atom method potential, parameterized to fit approximately the MD potential energies.²¹ If the potential energy increases between the initial and final states, the event occurs with reduced probability in order to satisfy microscopic reversibility,²³ otherwise, if the potential energy drops or remains constant, the event is performed with unit probability.

B. Binary collision model

The binary collision (BC) approximation describes the motion and interaction of energetic particles with the atoms of the film or substrate by a series of two-body collisions. To describe the two-body interaction, we follow closely the classical theory and approximation from Ref. 24. Asymptotic trajectories of the projectile and target atoms are computed considering elastic collisions. We use a purely repulsive Born–Mayer potential to describe their interaction because of its simplicity and the availability of potential parameters for a large variety of materials:

$$V(r) = A e^{-r/a}, \quad (1)$$

where A and a depend on the nature of the target and the projectile atoms.²⁴ When they are different species, a combination rule of the parameters is used:²⁴

$$A_{XY} = (A_{XX}A_{YY})^{1/2}, \quad a_{XY} = \frac{2a_{XX}a_{YY}}{a_{XX} + a_{YY}}, \quad (2)$$

where A_{XY} and a_{XY} are the parameters entering Eq. (1) for collisions of an atom of type X with an atom of type Y . The subscripts XX and YY correspond to the parameters for collisions of atoms of the same type. In the following, *initial* is related to quantities before collision (e.g., kinetic energy of the projectile) while *final* characterizes quantities resulting from the collision (e.g., kinetic energy of an atom initially at rest). The collision sequence obeys some basic rules.

Collisions with atoms having impact parameters (smallest distance to the extended straight line trajectory) larger than a characteristic distance b_{max} are not included. The first collision with a film or substrate atom is determined by the first time the trajectory reaches a point where $b < b_{\text{max}}$. b_{max} is a parameter linked to the number of collisions in a cascade, and is adjusted to fit experimental measurements of sputtering yields.

If the final kinetic energy of the atom initially at rest is larger than U_{thr} , the atom becomes a new projectile atom and is considered for a sequence of binary collisions. The energy U_{thr} corresponds to the kinetic energy to move an atom from its position in a lattice site. This energy depends on the local configuration, e.g., surface atoms require less energy to leave their lattice sites than bulk atoms. We assume that the value U_{thr} scales with the binding energy of the atom to the site, i.e.,

$$U_{\text{thr}} = \frac{V_{\text{binding}}}{V_{\text{bulk}}} U_{\text{thr bulk}}, \quad (3)$$

where V_{binding} and V_{bulk} are, respectively, the binding energies of the atom in its initial position and in a bulk site. $U_{\text{thr bulk}}$ is the threshold energy to extract an atom from its bulk lattice position and empirical values are available for different materials.²⁴ Because of the low kinetic energy of impinging particles on the surface and the high $U_{\text{thr bulk}}$, only surface atoms are capable of leaving their lattice site. Considering that in a typical event, an atom leaves a step position to form an adatom on the surface, the difference between these configurations is about equal to the adatom formation energy on the surface U_{ad} . This energy is subtracted from the kinetic energy of the recoil atom. Although an atom with a high coordination number is less likely to be displaced because of the difficulty of moving between closely spaced neighbors, this effect is accounted for by the subsequent collisions along the new trajectory.

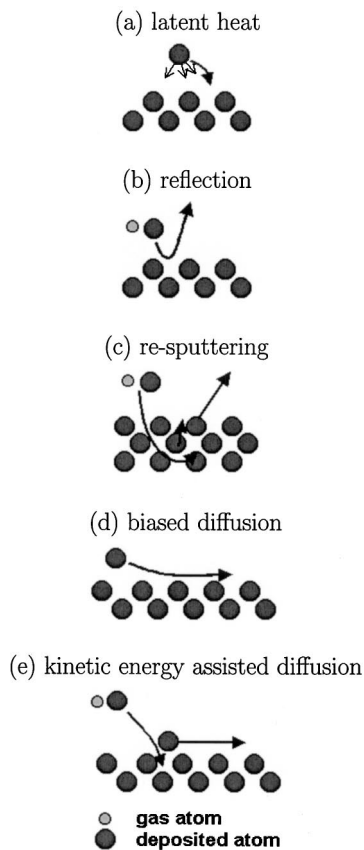


FIG. 4. The different surface mechanisms considered in the deposition model.

If the final kinetic energy of one of the projectile atoms is lower than a second threshold energy U_{stop} , the atom is stopped and is placed at a vacant site in the neighborhood. This is accomplished by searching the neighborhood of the atomic position up to the sixth nearest neighbor site. This distance is sufficient to find a place to put the vast majority of the projectile atoms, and adequately represents the actual system where it diffuses as an interstitial until it reaches an empty site. When the last atom stops, the MC thermal surface diffusion commences.

If the energetic particles collide with the atoms constituting the initial substrate, the projectile atom is stopped and a vacant site is sought near the impact position.

C. Specific surface mechanisms

Some additional mechanisms are included in the model of energetic collisions to account for those observed in MD simulations^{6–9}—latent heat of condensation, reflection, re-sputtering, biased diffusion, kinetic energy assisted diffusion—and are presented in Fig. 4. Note that reflection and re-sputtering are already described by the basic BC procedure, but changes of the particle trajectory resulting from their interaction with the surface are considered in this part.

Latent heat of condensation corresponds to the energy difference of the system when an atom passes from the vapor to a site on the surface. MD simulations show that 60%–70% of this energy is transformed into kinetic energy of the im-

pinging atom.⁶ It is the result of the attractive force exerted by the surface atoms on the impinging atom [Fig. 4(a)]. The Born–Mayer interatomic potential does not contain any attractive part. Thus we include this effect by adding a velocity component to the atoms passing near the surface, increasing their kinetic energy by U_{surf} . This velocity change is directed toward the closest atoms.

We apply similar rules to the atoms emitted from the surface. We compute the normal component of the velocity with respect to the closest surface atoms. If the kinetic energy corresponding to this velocity is larger than U_{emit} , the atom can escape the attraction of the surface, but it is emitted with a velocity reduced by this normal component. Resputtering or reflection particle energies [Figs. 4(b) and 4(c)] are also reduced by this surface emission energy. These effects are not relevant to Ar atoms because of their weak bonding to other atoms. If the energy corresponding to the normal velocity of an atom escaping the surface is lower than U_{emit} , the atom is reflected toward the surface. An atom impinging on the surface at grazing incidence can be trapped by the surface and diffuse over large distances in this way [biased diffusion in Fig. 4(d)]. Biased diffusion is highly directional.

Collisions of impinging atoms with the surface can induce diffusion of an atom already present on the surface; this is referred to as kinetic-energy-assisted diffusion in Ref. 7. As a result of the collision, adatom migration is not isotropic and takes place along a given direction. Various conditions have to be satisfied for such a displacement to occur. The final kinetic energy of such an atom must be lower than U_{thr} , otherwise it will become a free atom. Second, its kinetic energy must be larger than a threshold energy for kinetic-energy-assisted diffusion U_{kin} ($U_{\text{kin}} < U_{\text{thr}}$, U_{kin} takes values typical of diffusion energy barriers). If these conditions are satisfied, the next site along the trajectory is identified. If this empty site has higher or equal coordination, the atom can diffuse in this direction. The motion towards sites of lower coordination would present a significant increase of potential energy and would make the event less likely. Note that a thermal spike near the impact position may induce random diffusion jumps, but these are not included in this model.⁶

This BC based deposition model uses a set of parameters that we discuss below.

IV. SIMULATION RESULTS OF TA SPUTTERING

A. Simulation parameters of Ta sputtering deposition

We use in our model parameters appropriate to simulate tantalum deposition. Only a few energetic parameters (diffusion barriers and potential energies of adatoms on different faces) are known: activation energies of 0.78 and 0.5 eV for adatom diffusion on Ta bcc {100} and {110} orientations are taken from Ref. 25. MD simulations indicate activation energies of 0.44 eV for diffusion on Ta bcc {110} and 1.4 eV on Ta bcc {100} (through an exchange mechanism).²⁶ Note that the embedded atom method potential used in the MD showed good agreement with first principle calculations.²⁶ These high values of the activation energies for diffusion imply minimal surface diffusion at room temperature. Under these conditions, growth is isotropic for all orientations and inde-

pendent of the crystal structure.²⁷ The kinetic energy of impinging particles causes surface diffusion, and this process does not seem to restore any growth anisotropy: no sign of this process is present in the high resolution TEM images (Fig. 3), e.g., faceting is not observable. Based on these observations, neither orientation nor crystal structure nor deposition rate should be relevant in the simulations; the growth kinetics are governed mainly by the energetic processes on the surface. These observations allow further simplifications of the MC model and its parameterization.

(1) Sputtered Ta is known to produce bcc-Ta, β -Ta, or even fcc-Ta in evaporated very thin films of a few tens of Å.²⁸ In our experiments, bcc-Ta dominates¹⁵ but is likely to be mixed with some β phase. There is some evidence that β -Ta has a structure more close-packed than the simple bcc structure.²⁹ We use an fcc structure in our modeling (more close-packed than bcc), however, we believe that the influence of the crystal structure is weak as already mentioned. (2) We assume a deposition rate of 1 $\mu\text{m}/\text{min}$. (3) The substrate consists of an (001) atomic layer containing 100×100 atoms. Periodic boundary conditions are applied in the lateral dimensions of the simulation cell. Note that we do not simulate explicitly the native oxide formed on the silicon substrate in the experiments. Since Ta is a refractory material with low surface mobility, we expect that the deposited Ta atoms stick near their landing position independently of the substrate nature. (4) We use adatom diffusion barriers of 0.5 eV on the flat fcc {111} faces, and 0.78 eV for the other surface atoms, including step edges and similar configurations. Because of the high barriers the simulations are insensitive to the precise values. In this way, all the migration energies are equal or larger than those on the bcc {110} Ta fastest diffusion face. The Monte Carlo embedded atom method potential for Ta is obtained from the Al potential function²¹ that has been scaled to reproduce the Ta cohesive energy. However, simulations are insensitive to the detail of the potential energy calculation because of minimal surface diffusion.

In the deposition procedure, the impinging particles on the growing film are either Ar or Ta atoms. We use the same angular distribution for the two species.⁴ However, kinetic energies are different. Argon does not bond to the film, and so the desorption probability of Ar is 1. The parameters used in the BC model are summarized in Table I.

The adatom formation energy is subtracted from the kinetic energy of the recoil atoms. We use an adatom formation energy $U_{\text{ad}} = 3$ eV. This value is estimated by scaling adatom formation energies in Al (~ 0.2 – 1 eV for different faces²¹) by the ratio of melting temperature between Ta and Al (3269 K/933 K ~ 3.5). The scaling with melting temperature is well suited for bulk vacancy formation energy³⁰ (2.2–3.1 eV for Ta and 0.6–0.8 eV for Al in Ref. 31). This scaling likely (over) or (under) estimates surface defect energies. It should be noted that we do not introduce different parameters for the different crystalline orientations, even if the adatom formation energy varies on the different faces. This simplification is supported experimentally by the indication of isotropic growth (i.e., no facets) observed by TEM.

TABLE I. Summary table of the parameters used in the binary collision model.

Binary collision parameters		Reference
$A_{\text{Ta-Ta}}$ (keV)	53.133	24
$A_{\text{Ar-Ar}}$ (keV)	6.9609	24
$A_{\text{Ar-Ta}}$ (keV)	19.232	Eq. (2)
$a_{\text{Ta-Ta}}$ (Å)	0.2855	24
$a_{\text{Ar-Ar}}$ (Å)	0.2758	24
$a_{\text{Ar-Ta}}$ (Å)	0.2806	Eq. (2)
b_{max} (Å)	3.3	
U_{stop} (eV)	1	
U_{ad} (eV)	3	
$U_{\text{thr bulk}}$ (eV)	32	
U_{surf} (eV)	6	
U_{emit} (eV)	8	
U_{kin} (eV)	2	

The surface energy U_{surf} intended to describe the latent heat effect is set to 6 eV ($\sim 70\%$ of the Ta cohesive energy). U_{emit} is chosen at a significantly higher energy of 8 eV. $U_{\text{emit}} > U_{\text{surf}}$ accounts for the fact that atoms often come out from subsurface layers and must be extracted from a position with many surrounding neighbors.

The kinetic energy assisted diffusion mechanisms have been examined using MD calculations:⁶ if the atom trajectory is close to the minimum barrier diffusion path, an energy of about 1.3–1.7 times the thermal diffusion barrier is necessary to produce the diffusion. On Ta{100}, this barrier is 0.78 eV and we chose therefore $U_{\text{kin}} = 2$ eV for all diffusing directions. Again, it should be noted that for the sake of tractability, we do not introduce different parameters for the different crystalline orientations.

Using our BC model with these parameters, we have checked the sputtering yield of a single crystal Ta target under 100 and 400 eV Ar bombardment. These sputtering yields are usually considered as independent of temperature. We construct a 150×150 Å² and 50 ML thick Ta slice with periodic boundary conditions applied in the lateral directions. 5000 Ar atoms are projected on this target. We obtain sputtering yields $Y(100 \text{ eV}) \sim 0.2$ and $Y(400 \text{ eV}) \sim 0.8$ with our model in acceptable agreement with experimental sputtering yields $Y(100 \text{ eV}) \sim 0.1$ to 0.2 and $Y(400 \text{ eV}) \sim 0.5$ reported in Ref. 32.

B. Simulations of energetic particle effects

We consider a monoenergetic flux of Ta and Ar particles on the growing film. The average kinetic energy of the impinging atoms were estimated by Rossnagel *et al.* using a binary collision model (TRIM).⁴ In the case of 400 eV Ar impinging on the target, they found that the sputtered Ta atoms had an average kinetic energy of $T \sim 26$ eV, and the reflected Ar atoms had $T \sim 120$ eV while 25% of the Ar were reflected on the target toward the deposited film. TRIM is based on BC theory which is known to lose accuracy at low energies since it omits multibody interactions. We compared SRIM2000 (TRIM-like model³³) and TRIM calculations with molecular dynamics simulations. SRIM2000 calculations with default parameters showed a tendency to overestimate the

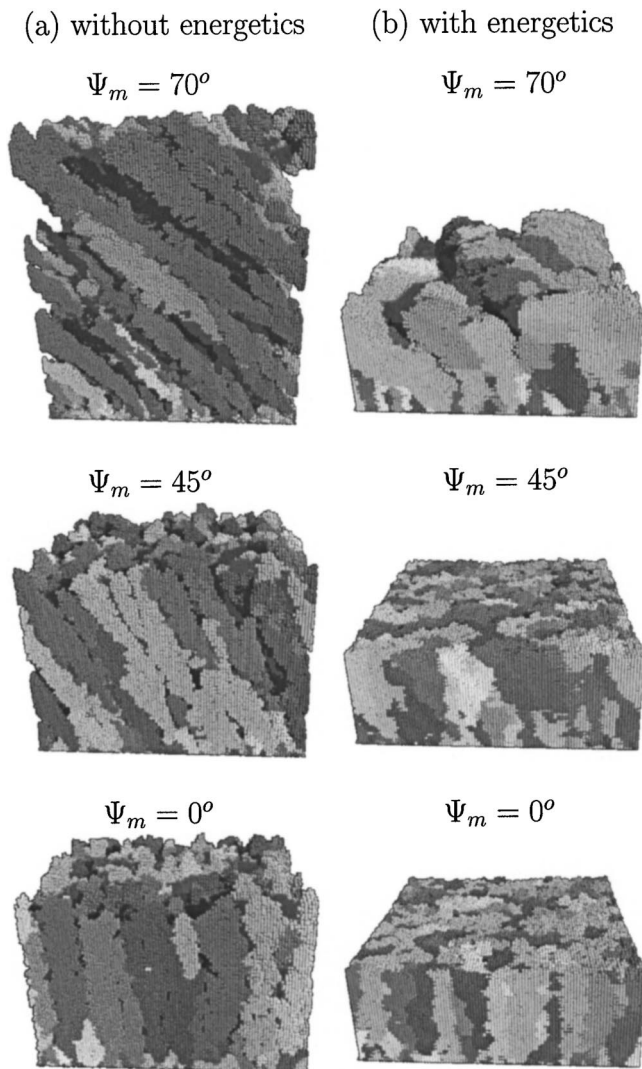


FIG. 5. Ta film morphology after 50 ML deposition at 300 K on different oriented substrates ($\Psi_m = 0^\circ, 45^\circ, 70^\circ$): (a) The effect of energetic particles are not included. (b) Energetic particles are considered. Ta and Ar initial kinetic energy are 10 and 50 eV. Ar atoms constitute 20% of the impinging particle flux. The shades of gray were introduced to help distinguish different columns. An atom alone on the substrate will be assigned a random gray scale and take the gray scale of one of its neighbors otherwise. An area of $300 \times 300 \text{ \AA}^2$ is displayed.

average kinetic energy of Cu sputtered by 400 eV Ar (Cu average kinetic energy ~ 18 eV) compared to molecular dynamics simulations ($\sim 8 \text{ eV}^{34}$), while the agreement between SRIM2000 and TRIM⁴ was good for Ta. In the absence of MD results for Ta sputtering, we used for a comparable sputtering voltage an average kinetic energy of 10 eV for Ta and 50 eV for Ar for impinging particles on the substrate (about half the TRIM predictions) and 20% are Ar atoms. These kinetic energies of impinging particles were able to reproduce experimental results in our simulations. In Fig. 2, we plot the density calculated in the film as a function of substrate inclination (the density in a layer is the ratio of occupied sites over total number of sites in the layer). Simulated morphology results are presented in Figs. 5(a) and 5(b) as a function of substrate inclination, with and without including the binary collision deposition model for the energetic par-

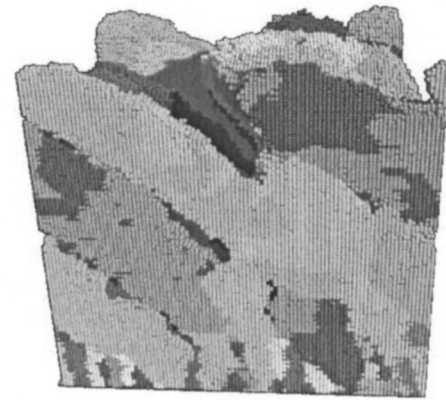


FIG. 6. Ta film morphology after 100 ML deposition at 300 K and at 70° substrate inclination. An area of $300 \times 300 \text{ \AA}^2$ is displayed. 50 ML have been added to the simulation presented in Fig. 5(b), $\psi_m = 70^\circ$. The shades of gray were introduced to help distinguish different columns. An atom alone on the substrate will be assigned a random gray scale and take the gray scale of one of its neighbors otherwise.

ticles. Without energetic particles, the film is rough and underdense, particularly at large substrate inclination. The density varies between ~ 0.6 and 0.3 in the range of Ψ_m considered. Comparison with experimental results gives large discrepancies, especially at large substrate inclinations. In contrast, with $T = 10$ eV for the Ta, $T = 50$ eV for the Ar, the density agrees very well with the experiments. Between 0° and 45° , the film is smooth and its density is close to 1. At 70° , the film exhibits a columnar structure but is more dense and smooth than without energetic particles. The morphology of simulated films at a substrate inclination of 70° are reported in Fig. 6 and can be compared to experimental results in Fig. 3. 100 ML are deposited. Simulated morphologies (Fig. 6) agree qualitatively with the HRTEM results: density, column size ($\leq 100 \text{ \AA}$), and a thin high density layer near the substrate are all well reproduced in the simulations.

C. Mechanisms affecting the film density

We wish to determine the main mechanisms responsible for the different densities observed in Figs. 5(a) and 5(b). We consider a 70° substrate inclination, we turn on different mechanisms in the simulations, and compare the film densities with the experiments. (1) Without energetic particles, the film density is ~ 0.3 [Fig. 5(a) and Fig. 2 (\diamond), $\psi_m = 70^\circ$]. This density is too low by more than 50%. (2) Latent heat effects are included, i.e., the initial kinetic energy of Ta is 0 ($T = 0$ for Ar) but increases up to a kinetic energy $T = 6$ eV when it collides with the surface. Latent heat alone causes a large increase of the film density up to ~ 0.5 [Fig. 2 (\square)]. (3) Considering an initial Ta kinetic energy of 10 eV ($T = 16$ eV at the surface as a result of latent heat, and the Ar kinetic energy is 0 eV) causes an increase of the density up to 0.75 [Fig. 2 (+)] in good agreement with the experiments. (4) Finally, including the Ar kinetic energy (the Ar kinetic energy is 50 eV and the Ta kinetic energy is 10 eV) only produces small variations of the density [Fig. 2 (\triangle)] and morphology of the film. Note that we also simulate a Ta kinetic

energy of 0 (but latent heat effect is allowed) and an Ar kinetic energy of 50 eV. These simulations show a density close to case 2 (latent heat effect alone) and confirms the weak effect of Ar neutrals on the film density.

These results indicate that first, the atomic displacements resulting from energetic particles during sputtering have a dramatic effect on the microstructure and morphology of the film. Without these displacements in the Ta sputter simulation the density is too low by more than 50%. Furthermore, these displacements must be included in order to model any realistic vapor deposition process, since latent heat effects are always present.

Next, we have pointed out that bombardment of the surface by Ar affects weakly the film microstructure when compared to Ta bombardment. The maximum kinetic energy T_m that can be transferred by a projectile to a target initially at rest is given by²⁴

$$T_m = \frac{4A}{(1+A)^2} T_0, \quad (4)$$

with $A = m_2/m_1$. T_0 is the initial kinetic energy of the projectile, m_1 is its mass, and m_2 is the target atom mass. T_m corresponds to the case of an impact parameter $b=0$. An Ar-Ta collision with an initial Ar kinetic energy of 50 eV ($A \sim 181/40 \sim 4.5$) leads to $T_m \sim 0.6T_0 \sim 30$ eV. A Ta particle impinging on the surface with a kinetic energy of 10 eV in the gas phase collides the surface with a kinetic energy $T_0 = 16$ eV because of the latent heat. Each Ta atom brings potentially 16 eV for its own athermal diffusion on the surface while the Ar neutrals need an impact parameter near $b \sim 0$ to transfer a significant part of their kinetic energy to Ta atoms on the surface. In addition, the Ta flux is four times larger than the Ar flux. As a result, the Ar bombardment has a weak effect on the film density.

D. Kinetic energy of impinging particles

In the previous sections, we used a Ta kinetic energy of 10 eV and 50 eV for the Ar as input parameters for the simulations. The film density was slightly overestimated [Fig. 2(Δ)]. We have also investigated other parameters; for example, a kinetic energy of 5 eV for Ta and 25 eV for the Ar slightly underestimated the density [Fig. 2(∇)]. In our model, a Ta energy between 5 and 10 eV (Ar effect is weak) reproduces correctly the experimental density. However, the kinetic energies of impinging Ta and Ar that reproduce best the experimental film densities differ from the TRIM sputtering calculations⁴ (Ta 26 eV, Ar 120 eV). We can enumerate some reasons for this difference.³⁵

- (i) TRIM parameters are fit to high energy collisions, and may be inaccurate in the range of 500 eV and below.
- (ii) In these simulations an average kinetic energy is used for impinging particles on the film. The complete kinetic energy distribution might introduce differences.
- (iii) Our criteria for kinetic energy assisted diffusion may overestimate surface diffusion.

V. CONCLUSIONS

We have grown Ta thin films by magnetron sputtering onto oxidized Si substrates, and have varied the orientation of the substrate with respect to the growth direction from horizontal to near-vertical in order to simulate growth over steep topography. We find that:

- (1) from x-ray reflectance and atomic force microscopy, the film roughness increases, and the density decreases with orientation angle; and
- (2) HRTEM imaging also indicates an underdense structure comprising separated columns, even at low Ar pressure, with greater orientation angles resulting in lower density. Columns are less than 100 Å wide and do not show faceting on the top. This morphology indicates that growth is isotropic because of low surface mobility.

We have modeled the experimental results using Monte Carlo simulations, with conditions intended to approximate the experimental growth conditions, and with material parameters appropriate for Ta. We obtained the following results.

- (1) Examination of the film microstructure and morphology resulting from these simulations indicates that the energetics of impinging particles are necessary to adequately produce film densities comparable to those found experimentally. Without including these energetics, we are left with large discrepancies.
- (2) In contrast, we find good agreement using a simulated deposition procedure that includes a binary collision model to describe collisions of impinging Ta and Ar on the surface. This model describes the essential surface mechanisms that influence the local film structure: resputtering, reflection, latent heat, kinetic-energy-assisted diffusion, and bi-ased diffusion. Simulated microstructures are in agreement with the HRTEM pictures, i.e., column size, column shape, and a thin dense layer at the substrate are all reproduced.

(3) We find in particular that the energy release due to attractive interactions between the impinging Ta atoms and the film adatoms (i.e., latent heat) produces a large increase of density (from ~ 0.3 to 0.5) at 70° substrate inclination relative to the case in which no latent heat is included. We note that simulations of Ta sputter deposition that neglect this latent heat effect do not provide realistic film structures, even in the case of films grown under high Ar pressure.

(4) We investigate the relative effect of Ta and Ar bombardment of the surface. We find that Ar neutrals have weak effects on the film density when compared to Ta. A kinetic energy of the Ta within 5–10 eV provides the best agreement between our modeling and the experiments.

ACKNOWLEDGMENTS

This work was supported by a NSF/DARPA VIP contract through the University of Illinois and by the U.S. Department of Energy, Office of Sciences, Laboratory Technology Division under Contract No. DE-AC05-96OR22464 with Lockheed Martin Energy Research Corp. and Contract No. DE-AC05-76OR00033 with Oak Ridge Associated Universities. Some of this work was performed under the aus-

pices of the U.S. Department of Energy, at Lawrence Livermore National Laboratory under Contract No. W-7405-Eng-48, and from the Office of Basic Energy Sciences. This work was supported by Bell Laboratories, Lucent Technologies, LAAS-CNRS and Laboratoire de Physique des Solides-UMR5477.

- ¹R. N. Tait, S. K. Dew, T. Smy, and M. J. Brett, *J. Appl. Phys.* **70**, 4295 (1991).
- ²L. Abelmann and C. Lodder, *Thin Solid Films* **305**, 1 (1997).
- ³A. G. Dirks and H. J. Leamy, *Thin Solid Films* **47**, 219 (1977).
- ⁴S. M. Rossnagel, C. Nichols, S. Hamaguchi, D. Ruzic, and R. Turkot, *J. Vac. Sci. Technol. B* **14**, 1819 (1996).
- ⁵F. M. D'Heurle, *Metall. Trans.* **1**, 725 (1970).
- ⁶X. W. Zhou and H. N. G. Wadley, *Surf. Sci.* **431**, 42 (1999).
- ⁷X. W. Zhou and H. N. G. Wadley, *Surf. Sci.* **431**, 58 (1999).
- ⁸J. D. Kress, D. E. Hanson, A. F. Voter, C. L. Liu, X. Y. Liu, and D. G. Coronell, *J. Vac. Sci. Technol. A* **17**, 2819 (1999).
- ⁹D. E. Hanson, J. D. Kress, A. F. Voter, and X. Y. Liu, *Phys. Rev. B* **60**, 11 723 (1999).
- ¹⁰J. G. C. S. P. Ju, C. I. Weng, and C. C. Hwang, *J. Appl. Phys.* **89**, 7825 (2001).
- ¹¹X. W. Zhou and H. N. G. Wadley, *J. Appl. Phys.* **84**, 2301 (1998).
- ¹²A. F. Voter, *J. Chem. Phys.* **106**, 4665 (1997).
- ¹³R. A. J. Y. G. Yang and H. N. G. Wadley, *Acta Mater.* **45**, 1455 (1997).
- ¹⁴L. Wang and P. Clancy, *Surf. Sci.* **473**, 25 (2001).
- ¹⁵D. L. Windt, J. Dalla Torre, G. H. Gilmer, J. Sapjeta, R. Kalyanaraman, F. H. Baumann, P. L. O'Sullivan, D. Dunn, and R. Hull, *Mater. Res. Soc. Symp. Proc.* **564**, 307 (1999).
- ¹⁶D. L. Windt, *Comput. Phys.* **12**, 360 (1998).
- ¹⁷*Thin Film Processes*, edited by J. L. Vossen and W. Kern (Academic, San Diego, CA, 1978), p. 115.
- ¹⁸J. A. Thornton, *J. Vac. Sci. Technol.* **11**, 666 (1974).
- ¹⁹R. A. Roy and R. Messier, *J. Vac. Sci. Technol. A* **2**, 312 (1984).
- ²⁰H. Windischmann, *J. Vac. Sci. Technol. A* **9**, 2431 (1991).
- ²¹H. Huang, G. H. Gilmer, and T. Diaz de la Rubia, *J. Appl. Phys.* **84**, 3636 (1998).
- ²²H. Huang, T. Diaz de la Rubia, and G. H. Gilmer (unpublished).
- ²³G. H. Gilmer and P. Bennema, *J. Appl. Phys.* **43**, 1347 (1972).
- ²⁴W. Eckstein, *Springer Series in Material Science 10: Computer Simulation of Ion-Solid Interactions* (Springer-Verlag, Berlin, 1991).
- ²⁵A. Gonis, T. Lenosky, T. Diaz de la Rubia, G. H. Gilmer, W. H. Butler, N. Kiouisis, C. S. Shin, and J. E. Greene (unpublished).
- ²⁶P. Klaver and B. Thijssse, *Thin Solid Films* **2**, 467 (1968).
- ²⁷J. Dalla Torre, G. H. Gilmer, D. L. Windt, F. H. Baumann, R. Kalyanaraman, H. Huang, T. Diaz de la Rubia, and M. Djafari Rouhani, *Mater. Res. Soc. Symp. Proc.* **562**, 129 (1999).
- ²⁸R. B. Marcus and S. Quigley, *Thin Solid Films* **2**, 467 (1968).
- ²⁹A. Jiang, A. Yohannan, N. O. Nnolim, T. A. Tyson, L. Axe, S. L. Lee, and P. Cote, <http://arxiv.org/abs/cond-mat/0208122>.
- ³⁰F. Agullo-Lopez, C. R. A. Catlow, and P. D. Townsend, *Point Defects in Materials* (Academic, New York, 1988).
- ³¹*Atomic Defects in Metals, Vol. 25 of Landolt-Börnstein, New Series, Group III*, edited by H. Ullmaier (Springer-Verlag, Berlin, 1991).
- ³²N. Matsunami, Y. Yamamura, Y. Itikawa, N. Itoh, Y. Kazumata, S. Miyagawa, K. Morita, R. Shimizu, and H. Tawara, *At. Data Nucl. Data Tables* **31**, 1 (1984).
- ³³J. F. Ziegler and J. P. Biersack, *SRIM: the stopping and range of ions in matter*, <http://www.research.ibm.com/ionbeams/SRIM/SRIMLEGL.HTM>.
- ³⁴H. Gades and H. M. Urbassek, *Appl. Phys. A: Mater. Sci. Process.* **61**, 39 (1995).
- ³⁵We did not include in our discussion possible collisions of the energetic particles with the Ar gas in the chamber between the target and the substrate. Collisions may reduce the difference between our kinetic energy parameters and TRIM parameters. A rough estimate of the Ar and Ta mean free path L is given by $L = 1/(n\pi\delta^2)$, where n is the number of Ar by unit volume in the chamber and δ the interaction distance between colliding particles. At a pressure of 2 mTorr in the chamber, with $\delta \sim 3 \text{ \AA}$, a Ta-Ar collision gives $L \sim 5.5 \text{ cm}$. L takes values close to the target-substrate distance ($\sim 8 \text{ cm}$). A large number of Ta sputtered atoms collide with the Ar gas between the target and the substrate and reduce their average kinetic energy.

Journal of Applied Physics is copyrighted by the American Institute of Physics (AIP). Redistribution of journal material is subject to the AIP online journal license and/or AIP copyright. For more information, see <http://ojps.aip.org/japo/japcr/jsp>
Copyright of Journal of Applied Physics is the property of American Institute of Physics and its content may not be copied or emailed to multiple sites or posted to a listserv without the copyright holder's express written permission. However, users may print, download, or email articles for individual use.